Mechanisms of the adsorption of oxygen molecules and the subsequent oxidation of the reconstructed dimers on Si(001) surfaces

T. Hoshino

School of Science and Engineering, Waseda University, 3-4-1 Ohkubo, Shinjuku-ku, Tokyo 169, Japan

M. Tsuda and S. Oikawa

Laboratory of Physical Chemistry, Faculty of Pharmaceutical Sciences, Chiba University, Chiba 260, Japan

I. Ohdomari

School of Science and Engineering, Waseda University, 3-4-1 Ohkubo, Shinjuku-ku, Tokyo 169, Japan
and Kagami Memorial Laboratory for Materials Science and Technology, Waseda University,
2-8-26 Nishiwaseda, Shinjuku-ku, Tokyo 169, Japan
(Received 5 July 1994)

The adsorption of O_2 molecules on 2×1 reconstructed dimers on Si(001) surfaces and the subsequent oxidation have been investigated by *ab initio* quantum-chemical calculations. Detailed analyses of the potential-energy hypersurfaces in the spin triplet and quintet states have revealed that the triplet state has the lowest-energy reaction path of the oxidation process. On this lowest-energy reaction path, the electronic state as well as the atomic-level configuration of the molecularly adsorbed metastable precursor of O_2 on Si(001) surfaces was clarified. The molecular adsorbate is converted into the atomically adsorbed stable state by the dissociation of the O_2 adsorbate to oxygen atoms. This is just the insertion process of an oxygen atom into a Si dimer bond to produce silicon oxide. The activation energy required for this conversion has been calculated to be 60.4 kcal/mol, which is in accordance with the value 60 kcal/mol obtained by experiments at high temperatures. By the inspection of the temperature dependence of the reaction-rate constants, it has been concluded that the reconstructed dimer is hardly oxidized at room temperature and that the origin of the natural oxide of Si(001) surfaces might be defects of the surface reacting with O_2 molecules, i.e., the defect-free Si(001) surface is stable against O_2 molecules and is not oxidized at room temperature. This conclusion is consistent with recent experimental results that reconstructed dimers on the terraces of Si(001) surfaces were inactive for an exposure of O_2 molecules and only defect sites on the same surfaces have reacted with O_2 molecules.

I. INTRODUCTION

A great deal of research[1-12] has been devoted to analyses of the adsorption and reaction of O_2 molecules on the surfaces of single crystal silicon. The interest has been concentrated on the determination of the chemical species of oxygen in the adsorption process, i.e., molecular or dissociative (atomic). Many trials to determine the precise structures of oxygen adsorbed Si surfaces have been performed.

With respect to the Si(111) surface, Hofer and co-workers[1,2] clarified the existence of a molecularly adsorbed metastable precursor of O_2 using several spectroscopic techniques. They also clarified that this precursor was converted to a dissociated final stable state of oxygen through a thermally or electronically activated process, and the activation energy in this process was estimated[2] to be 5.5 kcal/mol on 7×7 surfaces. Hollinger *et al.*[3] also detected conversion from the molecular precursor of adsorbed oxygen on Si(111) surfaces to the final stable state using synchrontron radiation photoemission spectroscopy. Silvestre and Shayegan[8] verified the existence of an oxygen precursor by measurements of the work-function shift of Si(111) surfaces, which originate from an

O_2 gas exposure on the surface at low temperatures ($T \simeq 20$ K). They also observed that this precursor was stable at low temperatures ($T < 120$ K), and that the activation energy for the conversion of this precursor to a stable state was very low, i.e., 0.9 kcal/mol.

For Si(001) surfaces, a similar adsorption process, i.e., the conversion from a molecularly adsorbed metastable precursor to a dissociated final stable state of oxygen, was also suggested by several studies.[9-12] However, the process remains obscure for Si(001) surfaces, and the activation energy for the conversion from the precursor to the stable state has not yet been reported explicitly.

A theoretical approach to the adsorption and subsequent reaction of O_2 molecules on Si surfaces has not been developed enough. Semiempirical and nonempirical quantum-chemical calculations by Barone[13] or Smith and Wander[14] gave just the stable structures of the final oxides. First-principles total-energy calculations with the local-density approximation by Miyamoto and co-workers[15] failed to find even the existence of an activation energy barrier for the dissociation process of the O_2 molecule on the Si surface.

The main target of this research is the elucidation of the reaction mechanisms of the oxygen adsorption and

the subsequent oxidation processes on Si(001) surfaces, which reproduce experimental findings. A short description of the method used in this study and the results are presented in Secs. II and III, respectively. In Sec. IV, a discussion is given comparing the results with experimental findings. Finally, the results are summarized, and conclusions are given, in Sec. V.

II. METHOD OF CALCULATIONS

A. Computational procedures

The potential-energy hypersurface for the adsorption reaction of O_2 molecules on the Si(001) surface was determined using the ab initio molecular-orbital (MO) method with the Møller-Plesset (MP) perturbation theory, which is an advanced method beyond the Hartree-Fock (HF) level calculation, because electron correlation is taken into account.[16]

Hartree-Fock level calculations

In the HF method, the eigenvalue equation for the electronic state is reduced into the one-electron eigenvalue equation

$$f(x)\psi_i(x) = \varepsilon \psi_i(x) ,$$

$$f(x) = -\tfrac{1}{2}\nabla^2 - \sum_{a=1}^{v} \frac{Z_a}{r_a} + \sum_{j}^{N} \{J_j(x) - K_j(x)\}$$

$$= h(x) + v^{HF}(x) \quad \left[h(x) = -\tfrac{1}{2}\nabla^2 - \sum_{a=1}^{v} \frac{Z_a}{r_a} \right] ,$$

$$J_j(x)\psi_i(x) = \left[\int dx' \psi_j^*(x') r^{-1} \psi_j(x') \right] \psi_i(x) ,$$

$$K_j(x)\psi_i(x) = \left[\int dx' \psi_j^*(x') r^{-1} \psi_i(x') \right] \psi_j(x) ,$$

(1)

where N and v are the total number of electrons and nuclei, respectively, x and x' are the position vectors of each of two electrons, and r is the distance between them. r_a is the distance between the electron x and the nucleus a. Z_a is the atomic number of the nucleus a and ψ_i are the molecular orbitals (MO's). The wave function of the ground electronic state of a molecule is expressed by a single Slater determinant constructed by the eigenfunctions obtained from Eq. (1). Since the operator $f(x)$ in Eq. (1) depends on its solution $[\psi_j(x')]$ thorough the electron-interaction terms (J_j and K_j), the eigenvalue equation (1) must be solved iteratively. The Hartree-Fock (HF) energy E of the ground electronic state is given in the following expression:

$$E = \sum_i^N \left\langle \psi_i(x) \left| -\tfrac{1}{2}\nabla^2 - \sum_{a=1}^{v} \frac{Z_a}{r_a} \right| \psi_i(x) \right\rangle$$

$$+ \tfrac{1}{2} \sum_i^N \sum_j^N \langle \psi_i(x) | J_j(x) - K_j(x) | \psi_i(x) \rangle . \quad (2)$$

Second-order perturbation-theory calculations

In the MP perturbation approach, the true Hamiltonian H for the electronic state is partitioned into two parts,

i.e., H_0 and the perturbed term V:

$$H = H_0 + V ,$$

where

$$H = \sum_i^N h_i(x) + \sum_{i=1}^{N} \sum_{j>i}^{N} r_{ij}^{-1} ,$$

$$H_0 = \sum_i^N f_i(x) = \sum_i^N [h_i(x) + v_i^{HF}(x)] , \quad (3)$$

$$V = \sum_i^N \sum_{j>i}^{N} r_{ij}^{-1} - \sum_i^N v_i^{HF}(x) .$$

The Rayleigh-Schrödinger perturbation theory using the partitioning of the Hamiltonian in Eq. (3) gives the HF energy [Eq. (2)] as the sum of the zeroth- and first-order energies. The correlation energy is first given by the second-order energy E_2 [Eq. (4)]:

$$E_2 = \tfrac{1}{4} \sum_i \sum_j \sum_m \sum_n \frac{\langle ij \| mn \rangle \langle mn \| ij \rangle}{\varepsilon_i + \varepsilon_j - \varepsilon_m - \varepsilon_n} , \quad (4)$$

where

$$\langle ij \| mn \rangle = \langle ij | mn \rangle - \langle ij | nm \rangle ,$$

$$\langle ij | mn \rangle = \int \int dx \, dx' \psi_i^*(x) \psi_j^*(x') r^{-1} \psi_m(x) \psi_n(x') .$$

ψ_i and ψ_j are the occupied MO's whereas ψ_m and ψ_n are the unoccupied MO's by electrons in the ground electronic state, i.e., the second-order energy correction by Eq. (4) is due to double excitations from the occupied MO's, and ψ_i and ψ_j are due to the virtual MO's ψ_m and ψ_n. ε_i, ε_j, ε_m, and ε_n are the eigenvalues of the eigenfunctions ψ_i, ψ_j, ψ_m, and ψ_n, respectively, determined from Eq. (1).

Minima and saddle points on the potential-energy hypersurface are characterized by the first and second derivatives of the potential energy with respect to the mass-weighted coordinates of the nuclei. The first derivatives with respect to all of the coordinates of the nuclei must be zero at a local minimum or a saddle point. If all the second derivatives on vibrational modes are positive, the point is a local minimum. On the other hand, only one of the second derivatives is negative and all others are positive at a saddle point. When some atoms of the considered molecule were fixed at their initial positions during computations, the derivatives with respect to these fixed atoms were omitted from the conditions for minima and saddle points. In order to determine the minima and saddle points, the optimization method developed by Schlegel[17] was employed. Most calculations have been performed with GAUSSIAN92 computation program produced by Gaussian, Inc.

B. Model molecular systems

Figure 1(a) represents (2×1) reconstructed dimers on the ideal Si(001) surface. It has already been clarified[18] that the dimers become symmetric structures on an ideal Si(001) surface which is free from defects or impurities. Our previous study[19,20] revealed that there exist two

(a)

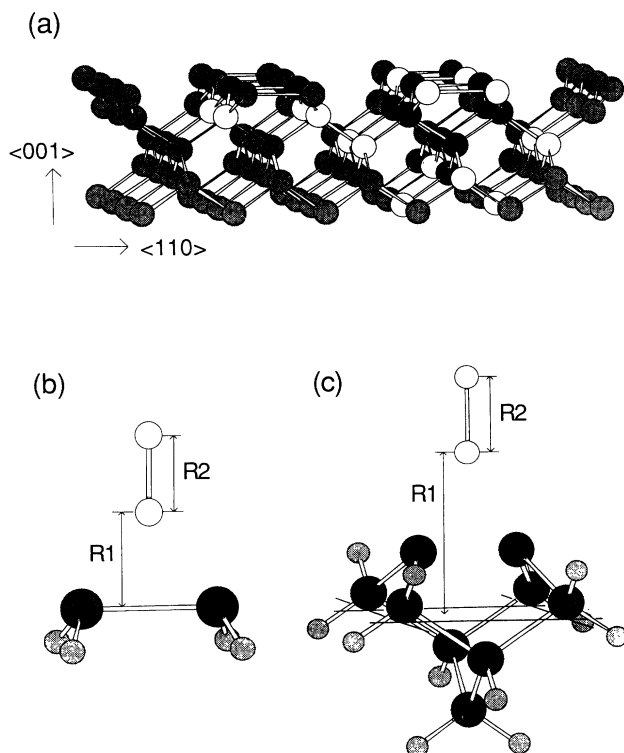

<001>

<110>

(b)   (c)

R2

R1

R2

R1

FIG. 1. (a) 2×1 reconstructed Si(001) surface. Solid and open spheres at the left were considered for the construction of a small model, and those at the right for a large model. (b) A molecular system of the small model, $Si_2H_4+O_2$. (c) A molecular system of the large model, $Si_9H_{12}+O_2$. Large and small solid spheres denote silicon and hydrogen atoms, respectively. Open spheres denote oxygen atoms in (b) and (c).

stable geometries when an O_2 molecule is adsorbed on a symmetric dimer. One is the case when the molecular axis of an O_2 molecule is perpendicular to a Si dimer bond, and the other is the case when the molecular axis is parallel. For the latter case, it has already been reported that the adsorption of an O_2 molecule to the Si dimer forms a Si-O-O-Si configuration with a stabilization energy of 41.8 kcal/mol (Ref. 20) and may give a scanning tunneling microscope (STM) image of a so-called missing dimer defect.[19]

In this paper, research was concentrated on the oxidation reaction mechanism which is generated in the former case, i.e., an O_2 molecule is inserted into a Si dimer in the fashion shown in Figs. 1(b) and 1(c), and subsequently dissociates to form silicon oxide.

Two types of model compounds—a small model [$Si_2H_4+O_2$, Fig. 1(b)] and a large model [$Si_9H_{12}+O_2$, Fig. 1(c)]—have been used in this study. In order to construct the model compounds usable for *ab initio* quantum-chemical calculations, first we focused on two atoms of a Si dimer and the second-layer atoms [see the left part in Fig. 1(a)]. The two atoms of the Si dimer (the solid spheres) were left unchanged, while the four second-layer atoms (the open spheres) were replaced by hydrogen atoms in the small model. The structure of this Si_2H_4 model is assumed to be the symmetric dimer part of the most stable atomic configuration of the large mod-

el, Si_9H_{12}, which is described below. The Si-H bond length of this model is 1.48 Å, which was taken from the optimized structure of the singlet SiH_2 molecule. The small model $Si_2H_4+O_2$ is employed for the preparation of detailed maps of the potential-energy hypersurfaces from which the most probable reaction paths of the Si dimer oxidation process were determined for the spin triplet as well as spin quintet electronic states.

The large model $Si_9H_{12}+O_2$ is employed for the purpose of the elaboration of the total-energy change along the most probable reaction path which was determined using the small model. In order to take the influence from the underlayer Si atoms into account, the large model consists of the part shown in the right side of Fig. 1(a). In a manner similar to that used in constructing the small model $Si_2H_4+O_2$, nine Si atoms (solid spheres) were left unchanged, and 12 outer atoms designated by open spheres were replaced by hydrogen atoms. The atomic configuration of the underlayer part of this Si_9H_{12} model was assumed to be a single-crystal structure of silicon, i.e., the Si-Si bond length and the bond angles are 2.35 Å and 109.47°, respectively. The Si-H bond length is 1.48 Å. The two uppermost Si atoms are allowed to move independently through the optimization. It will be suggested in Sec. III that these two uppermost Si atoms always keep a symmetric configuration through the oxidation reaction.

C. Basis set functions and electronic states

Each MO is expressed by a linear combination of Gaussian-type basis set functions. All calculations in this study are carried out with the standard split-valence-type basis set 3-21G.[21]

The ground electronic state of a symmetric dimer of Si is proved to be the singlet state.[22] The ground electronic state of an O_2 molecule is known[23] to be the spin triplet $^3\Sigma_g$, which is energetically more stable than the spin singlet state $^1\Delta_g$ by 22.5 kcal/mol and than the state $^1\Sigma_g$ by 37.5 kcal/mol, respectively (Fig. 2). Therefore, the ground electronic state of the total molecular system which consists of O_2 and a Si dimer is the triplet state. The first excited state of a symmetric Si dimer was proved[22] to be the triplet state, and the potential-energy level exists slightly above the ground state, as shown in Fig. 2. For this reason, we cannot ignore the possibility that the ground state of the total system might be the spin quintet state which arises from the $^3\Sigma_g$ oxygen and the silicon dimer in the triplet state. The calculations were performed for the following cases.

Case (1): the triplet O_2 molecule reacts with a singlet Si_2H_4 (the spin triplet state).

Case (2): the triplet O_2 molecule reacts with a triplet Si_2H_4 (the spin quintet state).

III. RESULT

A. Reaction mechanism in the triplet state [case (1)]

The potential-energy map for case (1), the spin triplet state, is shown in Fig. 3, where the abscissa (R_1) and or-
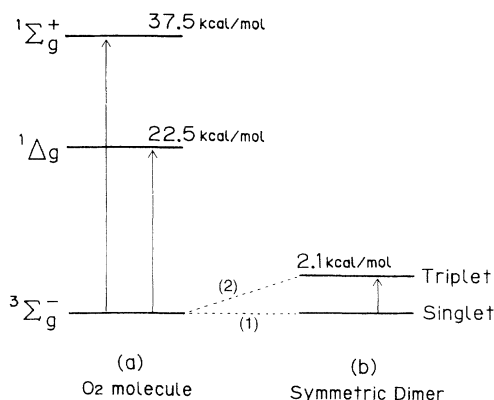
FIG. 2. Energy-level diagram of the electronic eigenstates for (a) an oxygen molecule and (b) a symmetric Si dimer. The total reaction systems in the spin triplet state (1) and the spin quintet state (2) originate from the combinations indicated by the dotted lines.

dinate (R_2) are the distances shown in Fig. 1(b), i.e., the distance (R_1) between the Si dimer bond and the lower oxygen atom and the bond length (R_2) of the reacting oxygen molecule, respectively. The total-energy calculations at the MP2 level were performed at more than 200 points to complete the potential-energy contour map (Fig. 3). The positions of the two Si atoms were fully optimized at every point of these more than 200 specified by the two variables R_1 and R_2, while four hydrogen atoms were always fixed at their initial positions to keep the crystal structure. The solid line in Fig. 3 denotes the lowest potential-energy path along the steepest potential gradient on the potential-energy hypersurface. The three minimum which indicates the physical adsorption of the O_2 molecule to Si(001) surfaces, (b) the transition state of the oxidation process of Si(001) surfaces by the O_2 molecule, and (c) the stable structure of silicon oxide that is finally produced.

When a spin triplet O_2 molecule is located far enough apart from a Si_2H_4 $(R_1=6$ Å$)$, both the Si_2H_4 and O_2 molecules keep their optimized structures which are determined in each standing alone, and the potential energy of the total reaction system is equal to the simple sum of each of them. Therefore, no interaction exists between them at $R_1=6$ Å. The value of the potential energy in this initial stage is set at the zero level of this contour map.

A shallow minimum appears when an O_2 molecule approaches the Si_2H_4 up to the distance of $R_1=4.30$ Å [Fig. 3(a)]. At this stage, the potential energy hardly changes along the R_1 direction, but a remarkable change is observed along the R_2. This situation means that the O_2 molecule keeps its molecular characteristics, and that the expansion or contraction of the O-O bond distance are strongly restricted at this stage (a). As shown in Fig. 4(a), the O-O distance keeps the same value as an isolated O_2 molecule, 1.24 Å, determined by the optimization with 3-21G basis set, and no charge transfer takes place between the Si_2H_4 and O_2 molecules. The alpha spin density which generates the spin triplet state in this calculation is localized completely at the oxygen part, and distributed equally in each of the oxygen atoms.

The potential energy of the system is elevated when the O_2 molecule approaches closer to the Si_2H_4. The O-O bond length R_2 begins to expand at the distance R_1 shorter than 2.5 Å. The potential energy increases gradually with the expansion of the bond length of the O_2 molecule. Figure 3(b) corresponds to the transition state of the oxidation reaction. The geometry and electronic structure [Fig. 4(b)] show that the O_2 molecule is just about to dissociate at point (b), i.e., the O-O bond length R_2 expands to 1.65 Å, and the alpha spin density begins to be localized at the upper oxygen atom. The electron transfer takes place from the Si_2H_4 to the O_2 molecule by $-0.3e$ at this transition state, and the distance R_1 is 2.12 Å. One should note that the alpha spin density at the upper oxygen atom changes drastically from 1.0 at point
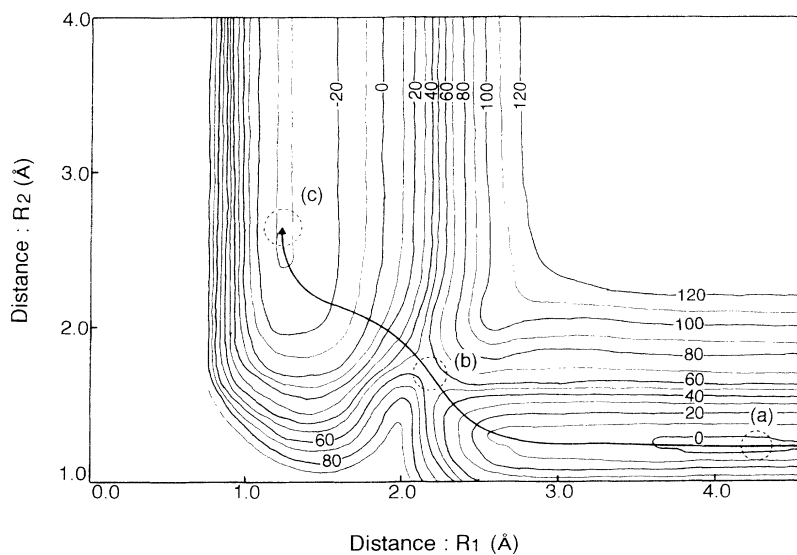

FIG. 3. Contour plots of the potential-energy hypersurface in case (1): the spin triplet state. The numerical values of the potential energy (kcal/mol) are indicated on the standard that the infinite separation between the Si dimer and the O_2 molecule is zero kcal/mol. Axes R_1 and R_2 correspond to distances R_1 and R_2 in Fig. 1(b). The solid line denotes the lowest potential-energy path along the steepest potential gradient on the potential-energy hypersurface. The three broken circles indicate (a) the shallow minimum, (b) the transition state, and (c) the final stable state of oxide. The potential-energy values and the atomic configurations were determined at the MP-2 level using the small model.

Distance : R1 (Å)

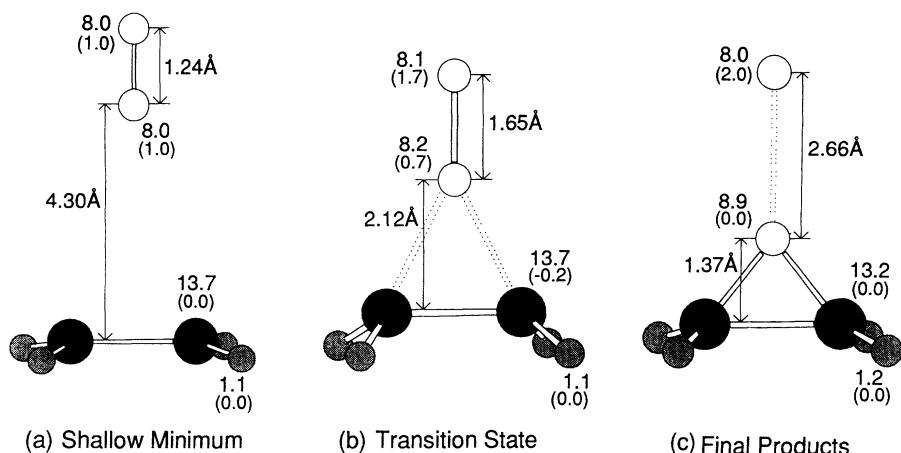(a) Shallow Minimum   (b) Transition State   (c) Final Products

FIG. 4. Atomic configurations for (a) the shallow minimum, (b) the transition state, and (c) the final stable state of the oxide in the spin triplet state, which correspond to (a), (b), and (c), respectively in Fig. 3. Electron densities and alpha spin densities (in parentheses) obtained by Mulliken population analysis are also shown.

(a) to 1.7 at point (b).

When the oxidation reaction proceeds beyond the transition state, a strong force appears to make the lower oxygen atom form chemical bonds with each Si atom. It should be noted that the potential-energy change depends only on R_1 and is independent of the O-O bond length R_2 in this area. This situation means that the O_2 molecule has already dissociated completely after passing through saddle point (b). Finally, the reaction system is stabilized at point (c), where silicon oxide and an oxygen atom are produced. This situation is reflected in the deep potential valley elongated along the R_2 axis in the potential-energy map in Fig. 3. The corresponding atomic configuration and the electronic structure are represented in Fig. 4(c). The generated silicon oxide is in the spin singlet state, whereas the atomic oxygen is in the spin triplet state, as shown by the alpha spin density of 2.0 at the upper oxygen atom. The electron transfer takes place from the Si atoms to the oxygen atom in the silicon oxide by $-0.9e$.

B. Reaction mechanism in the quintet state [case (2)]

The potential-energy map for case (2), the spin quintet state, is shown in Fig. 5. The shallow minimum corresponding to the physical adsorption (a), the transition state of the oxidation process of Si surfaces (b), and the stable structure of silicon oxide finally produced (c) exist in the quintet state in Fig. 5 similarly to the spin triplet state in Fig. 3. The solid line indicates the lowest potential-energy path along the steepest potential gradient on this potential-energy hypersurface.

When the spin triplet O_2 molecule and the spin triplet Si_2H_4 exist far enough apart from each other ($R_1 = 6$ Å), the structure of the reaction system retains the optimized structure which is obtained by the calculation on each of the isolated systems, and the potential energy of the total system is equal to the simple sum of these two isolated molecules. For this reason, the value of the potential energy at this initial state is assigned to the zero level of the potential-energy contour map in Fig. 5.
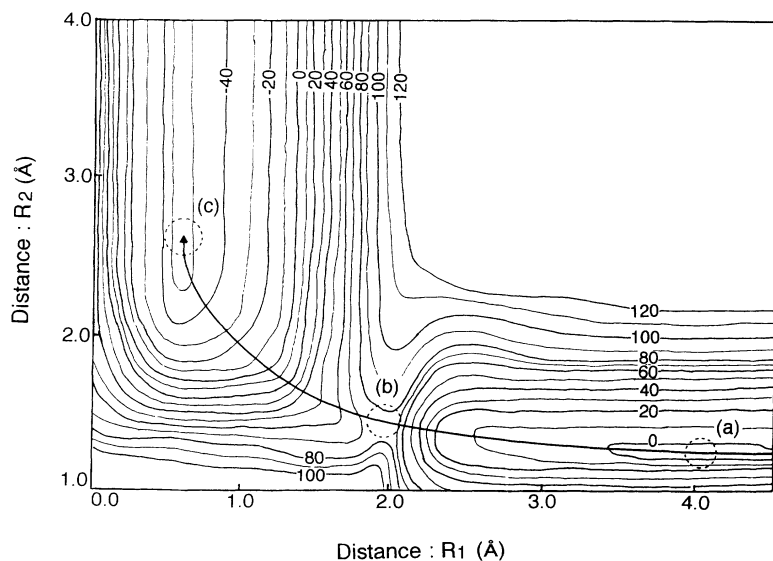

Distance : R1 (Å)

FIG. 5. Contour plots of the potential-energy hypersurface in case (2): the spin quintet state. The numerical values of the potential energy (kcal/mol) are shown on the standard that the infinite separation between the Si dimer and the O_2 molecule is 0 kcal/mol. Axes R_1 and R_2 correspond to distances R_1 and R_2 in Fig. 1(b). The solid line denotes the lowest potential energy path along the steepest potential gradient on the potential-energy hypersurface. The three broken circles indicate (a) the shallow minimum, (b) the transition state, and (c) the final stable state of oxide. The potential-energy values and the atomic configurations were calculated at the MP 2 level using the small model.

The reaction system is stabilized slightly when the O_2 molecule approaches the Si_2H_4 up to 4.02 Å [Fig. 5(a)]. The corresponding atomic configuration and electronic state are shown in Fig. 6(a). No charge transfer from the Si_2H_4 to the O_2 molecule occurs, and the O-O bond length (R_1) keeps the value of an isolated O_2 molecule, 1.24 Å, determined by the optimization with 3-21G basis set. Four alpha electrons, which originate the spin quintet state in this calculation, are distributed uniformly on each of the oxygen as well as silicon atoms. This situation means that the oxygen molecule still holds its characteristics as a molecule at this point.

The potential energy does not increase significantly until the O_2 molecule approaches the Si_2H_4 at about 3.0 Å, while the O-O bond length R_2 remains unchanged. Beyond 3.0 Å, the potential energy is elevated steadily while shortening the distance R_1, but the slight expansion of the O-O bond length r_2 still occurs. This situation in the quintet state is different from the spin triplet state, where a remarkable expansion of the O-O bond length R_2 was observed before the reaction proceeds to the transition state (Fig. 3). The transition state in the quintet state locates on point (b) in Fig. 5. The corresponding geometry and the electronic structure is shown in Fig. 6(b), where the O-O bond length R_2 is not so long: 1.40 Å, and the alpha spin density in the O_2 molecule is partly localized to the upper atom. This result indicates the generation of one oxygen atom in the spin triplet state (upper), and the other in the spin singlet state (lower).

Beyond the transition state, the O-O bond length R_2 begins to expand rapidly in accordance with the decrease of the potential energy. The system is finally stabilized at point (c), where silicon oxide and an oxygen atom are produced. No change of the potential energy against the distance R_2 indicates that the O_2 molecule has dissociated completely. The drastic change of the potential energy along the R_1 direction means that the oxygen atom forms strong chemical bonds with the Si atoms in the silicon oxide produced. As shown in Fig. 6(c), the silicon oxide with an Si-O-Si bridge configuration in the spin triplet state and an isolated oxygen atom in the spin trip-

let state are generated as the final products. A charge transfer occurs by $-1.0e$ from the Si atoms to the oxygen atom in the silicon oxide. The alpha spin density on the Si-Si dimer in Fig. 6(a) before the oxidation still remains on the same atoms even after the silicon oxide is generated [Fig. 6(c)].

C. The most probable reaction path

As shown in Fig. 3 for the spin triplet state and in Fig. 5 for the spin quintet state, two kinds of the lowest potential-energy paths along the steepest potential gradient were determined on the oxidation reaction of the outermost layer of the 2×1 reconstructed Si(001) surface. Which, then, is the most probable reaction path of the two? Since the absolute values of the potential energy on the zero level are different in each of the hypersurfaces, the potential energies appearing in Figs. 3 and 5 cannot be compared directly as they are. The difference in the absolute values of the potential energy in the infinite separation must be taken into consideration in the following discussion. Detailed comparisons of the potential-energy change following the reaction paths revealed that (1) the potential-energy hypersurface of the spin triplet state is lower than that of the quintet state at the infinite separation between an O_2 molecule and a Si_2H_4, and (2) the potential-energy hypersurface of the spin quintet state crosses with that of the spin triplet state only at the area of the final products. These findings indicate that the lowest potential-energy path of the spin triplet state is the most probable reaction path of the oxidation process of Si(001) surfaces with O_2 molecules. For this reason, it is concluded that the activation energy measured in experiments has to be generated in the reaction in the spin triplet state.

In order to determine theoretically an activation energy which is comparable with experiments, more elaborate calculations employing the large model $Si_9H_{12} + O_2$ were performed along the lowest potential-energy path in the spin triplet state. The result is shown in Fig. 7. The potential-energy change obtained following the lowest-
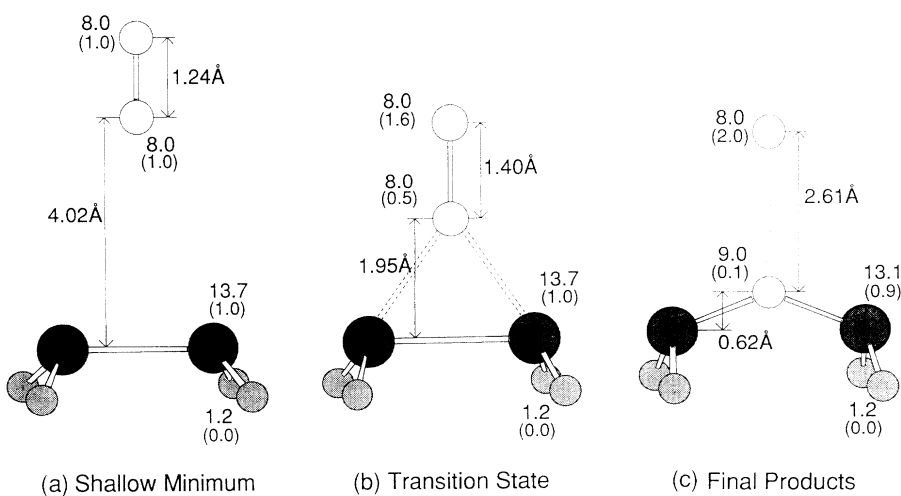

FIG. 6. Atomic configurations for (a) the shallow minimum, (b) the transition state, and (c) the final stable state in the spin quintet state, which correspond to (a), (b), and (c) in Fig. 5, respectively. Electron densities and alpha spin densities (in parentheses) obtained by Mulliken population analysis are also shown.
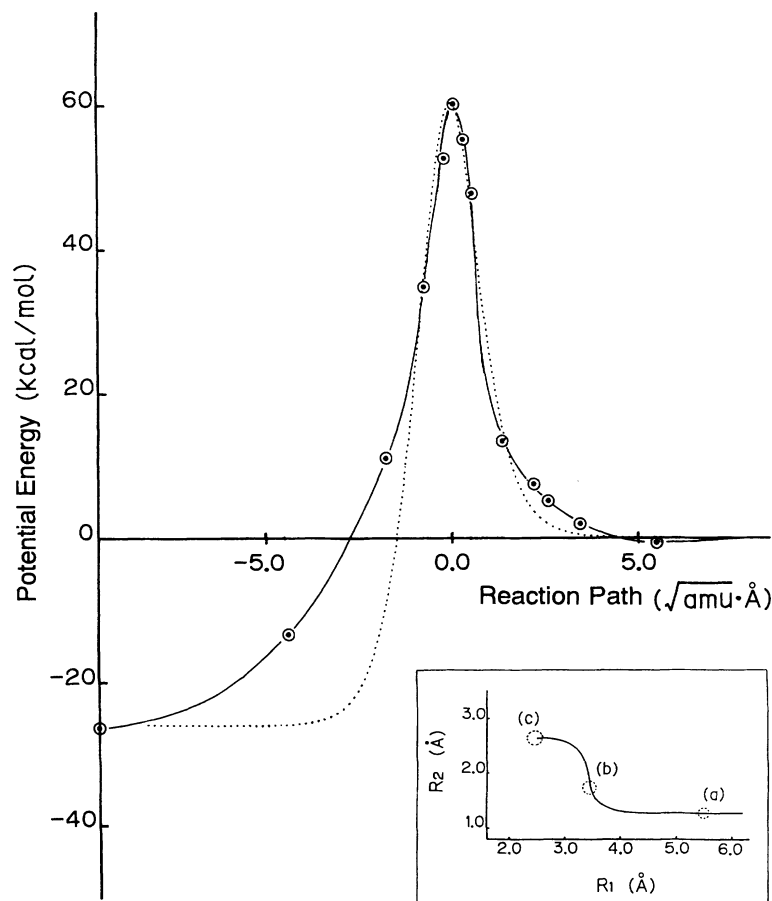
(a) Shallow Minimum   (b) Transition State   (c) Final Products

FIG. 7. The potential-energy change (kcal/mol) following the lowest energy reaction path ($\sqrt{\text{amu}}\cdot\text{Å}$) along the steepest potential gradient on the potential-energy hypersurface in the spin triplet state. The energy was calculated by the MP perturbation theory up to the second order using a large model: $Si_9H_{12}+O_2$. The zero line is the infinite separation between the Si dimer and the O_2 molecule. The distance on the abscissa is the reaction path on the potential-energy hypersurface expressed by the mass-weighted $3N$-6 dimensional Cartesian coordinates where N is 23, the number of the atoms constructing the large model. The inset shows the trace of the lowest-energy reaction path in the two-dimensional coordinates where distances R_1 and R_2 correspond to those of Fig. 1(c). The dotted line representing the Eckart-type potential-energy function was drawn by curve fitting performed in such a manner that these two potential-energy curves match well at the vicinity of the potential-energy barrier.

energy reaction path is shown as the solid line in Fig. 7. The oxygen bond length R_2 in Fig. 1(c) and the positions of two dimer Si atoms are fully optimized at the Hartree-Fock level at all the points in Fig. 7, specified by the distance R_1 between the Si(001) surface and the O_2 molecule which is shown in Fig. 1(c), while all the hydrogen atoms and seven underlayer Si atoms are fixed at their initial positions to retain the crystal structure. Using these optimized structures, the values of the potential energy were redetermined at the MP2 level.

The relationship between R_1 and R_2 following the lowest potential-energy reaction path is also shown in the inset of Fig. 7. Comparing the trace of the lowest potential-energy reaction path shown in Fig. 3 with those in Fig. 7, one can confirm the consistency of the computational results between the small $(Si_2H_4+O_2)$ and large models $(Si_9H_{12}+O_2)$. The shallow minimum, the transition state, and the final stable state are also recognized in Fig. 7. At the shallow minimum the system is stabilized by 0.6 kcal/mol. The potential energy at the transition state is very high, i.e., 60.4 kcal/mol, which is considered to be the activation energy required for this reaction. The stabilization energy of the final stable state is 26.4 kcal/mol. This small stabilization energy originates from the fact that the final products are the stable silicon oxide and the unstable oxygen atom.

IV. DISCUSSION

A. Temperature dependence of the oxidation reaction-rate constants

It is well known that Si(001) surfaces utilized for electronic devices are often covered with natural oxide thin films in air. However, the activation energy result obtained for the oxidation by O_2 molecules predicts that only the perfect (001) surfaces covered with the reconstructed dimers are not oxidized at room temperatures. What then, is the origin of the natural oxide formation?

It has generally been recognized[24-26] that the quantum-mechanical tunneling effect makes a significant contribution to chemical reactions (e.g., the hydrogen abstraction and insertion) and the effect appears dominantly in the rate constants at low temperatures. One of the most prominent effects induced by the tunneling is an unusual lowering of the apparent activation energy in experiments observed at low temperatures. For this reason, an investigation was carried out on the possibility of the contribution of the tunneling effect to the oxidation reaction which follows the adsorption of O_2 molecules on Si(001) surfaces at room temperatures. The lowering of the apparent activation energy in experiments could be predicted by the temperature dependence of rate con-

stants which are calculated with a consideration of the tunneling effect.

The barrier region of the lowest potential-energy reaction path (Fig. 7) has been fitted approximately to an analytical function of the Eckart potential.[27,28] The asymmetric Eckart potential along the reaction path x can be written as

$$V(x) = -A\xi/(1-\xi) - B\xi/(1-\xi)^2, \quad \xi = -\exp(2\pi x/L) \,,$$
(5)

where $-A$ is the exothermicity and L is a characteristic length related to the tunneling frequency. Using formula (5), the barrier height measured from the reactants is given by

$$V_{BH} = (A+B)^2/4B \,.$$
(6)

The result of a curve fitting with the Eckart potential is also shown in Fig. 7 by the dotted line. A particle having mass μ with translational energy (E_T) permeates through the Eckart potential barrier with a probability $P(E_T)$:

$$P(E_T) = 1 - \frac{\cosh[2\pi(\alpha-\beta)] + \cosh[2\pi\delta]}{\cosh[2\pi(\alpha+\beta)] + \cosh[2\pi\delta]} \,,$$
(7)

where

$$\alpha = \tfrac{1}{2}(E_T/c)^{1/2}, \quad \beta = \tfrac{1}{2}[(E_T-A)/c]^{1/2} \,,$$

$$\delta = \tfrac{1}{2}[(B-c)/c]^{1/2}, \quad c = h^2/8\mu L^2 \,.$$

h is the Planck constant. In the present theoretical analysis, the particle is the representative point of the reaction system on the potential-energy hypersurface, where $\mu = 1$ because the hypersurface is constructed with the mass-weighted coordinate as indicated in Sec. II A. A quantity proportional to the rate constant $k(T)$ is obtained by the following equation (8) with $P(E_T)$, when the Boltzmann distribution of the translational energies of the particle is assumed:

$$k(T) \propto \int_0^\infty P(E_T)\exp(-E_T/kT)dE_T \,.$$
(8)

The classical rate constant without the tunneling is also calculated in Eq. (8) by substituting the classical transmission probability $P^{CL}(E_T)$ with the quantum-mechanical $P(E_T)$:

$$P^{CL}(E_T) = \begin{cases} 0, & E_T < V_{BH} \\ 1, & E_T \geq V_{BH} \,. \end{cases}$$
(9)

In this classical case, Eq. (8) is integrated analytically to give the familiar form

$$k(T) \propto kT \exp(-V_{BH}/kT) \,.$$
(10)

The temperature dependence of the rate constants theoretically obtained using Eqs. (8) and (10) are shown in Fig. 8. The contribution of the quantum-mechanical tunneling effect appears in the rate constant at low temperatures. Nevertheless, the activation energy with the quantum-mechanical tunneling effect estimated from the local slope of the Arrhenius plot at low temperatures is still high: $\simeq 40$ kcal/mol. This result means that the
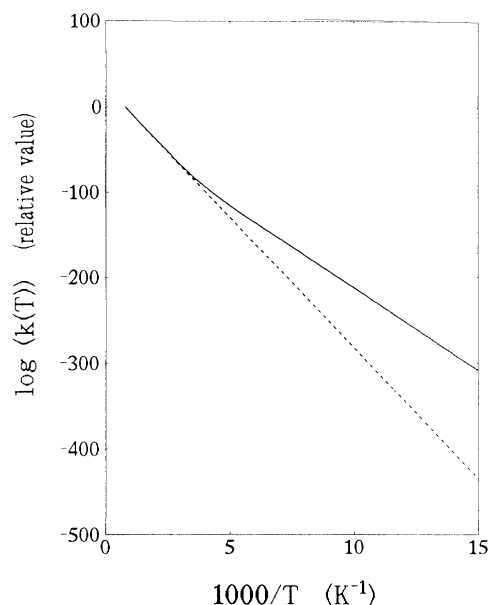

FIG. 8. Temperature dependence of the rate constants of the oxidation of the reconstructed Si dimers on Si(001) surfaces by O_2 molecules. The solid line represents the case considering the tunneling effect, and the dotted line expresses the classical case without quantum-mechanical tunneling. The rate constant at 1250 K was tentatively assumed to be unity at the ordinate.
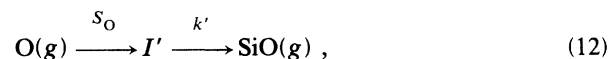
tunneling effect has no serious influence on the oxidation of Si(001) surfaces with O_2 molecules when the surface is perfectly covered with reconstructed dimers.

B. Comparison with experimental findings

Engstrom and co-workers[29,30] and Evelyn, Nelson, and Engel[31] used a pulse-modulated molecular-beam reactive scattering method in kinetic studies of O_2 molecules or oxygen-atom adsorption to Si(001) surfaces as well as Si_0 desorption from the same surfaces at high temperatures $(T > 1000 \text{ K})$. Their experimental results suggested the following sequential process in the reaction with molecular oxygen:

$$O_2(g) \xrightarrow{S_{O_2}} I_1 \xrightarrow{k_1} I_2 \xrightarrow{k_2} SiO(g) \,,$$
(11)
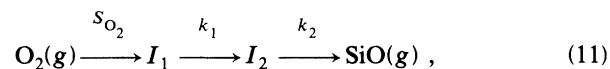
and for atomic oxygen:

$$O(g) \xrightarrow{S_O} I' \xrightarrow{k'} SiO(g) \,,$$
(12)

where S_{O_2} and S_O are the sticking probability of O_2 molecules and O atoms to Si(001) surfaces. The activation energies for the rate constants k_1 and k_2 were estimated to be 60 and 78.5 kcal/mol, respectively. The rate constant k' was found to be identical to k_2. Thus it was concluded that the adsorption of atomic oxygen directly generates the intermediate state I', and that I' in Eq. (12) is identical to the intermediate state I_2 in Eq. (11). This result was also confirmed by other groups[32,33] using similar modulated molecular-beam techniques. These results are strongly considered to support our theoretical results; i.e., the first step with k_1 in Eq. (11) is the oxidation pro-

cess of Si dimers by O_2 molecules adsorbed on Si(001) surfaces, and the second step with k_2 is the desorption of SiO from the surfaces. Moreover, it has been clarified from our theoretical research[34] that no activation energy is required in the oxidation of Si dimers on Si(001) surfaces by atomic oxygen, and that silicon oxide with the Si-O-Si bridging structure is formed spontaneously. Therefore, we conclude that the intermediate state I_2 in Eq. (11) is a final stable silicon oxide, and that the intermediate I_1 in Eq. (11) is a molecularly adsorbed precursor state and the rate constant k_1 corresponds to the oxidation process of a Si dimer on Si(001) surfaces by the adsorbed O_2 molecule. The activation energy 60.4 kcal/mol theoretically obtained by our calculations agrees quite well with the value derived from the modulated molecular-beam analyses.

Judging from the large activation energy estimated in this study, it is concluded that symmetric dimers on Si(001)-2×1 reconstructed surfaces are inert against the oxidation reaction by O_2 molecules and hardly oxidized at room temperatures. Recent STM observations by Avouris and Lyo[35] also support this conclusion. The STM images, after an exposure of O_2 molecules on Si(001)-2×1 surfaces, showed that the majority of symmetric dimers appearing were unreactive, while defect sites only, in particular C-type defects, have high reactivity and the oxidation of Si(001) surfaces at the initial stage is essentially restricted to the dimer defect sites. This high reactivity of C-type defects is reason why the conversion from the molecular precursor of O_2 adsorbed on Si(001) surfaces to the final stable state is not obviously detectable in experiments comparing with the cases for Si(111) surfaces.[9-12] The natural oxide film formation on Si(001) surfaces might originate from the defect sites.

Some groups reported[36,37] that electron transfer from Si surfaces to O_2 adsorbed molecules promotes the oxidation reaction on Si surfaces. This experiment is compatible with our calculation that the oxidation of reconstructed dimers on Si(001) surfaces by an adsorbed O_2 molecule requires a charge transfer of 0.3 electrons at the transition state in the spin triplet state [Fig. 4(b)].

V. SUMMARY

The adsorption reaction of O_2 molecules and the subsequent oxidation of reconstructed dimers on Si(001) surfaces were investigated using *ab initio* quantum-chemical calculations. The investigation has been performed both in cases of spin triplet and spin quintet states. For both cases, detailed analyses using potential-energy contour maps revealed that (1) a shallow minimum of the potential-energy hypersurface exists for the molecular adsorbate of O_2 on Si(001) surfaces as a precursor, (2) the dissociation of the adsorbed O_2 molecule for the oxidation of Si(001) surfaces requires a large activation energy, and (3) silicon oxide with an Si-O-Si structure and an isolated oxygen atom are generated as the reaction products.

The lowest-energy reaction path exists on the potential-energy hypersurface in the lowest triplet state. The activation energy for the oxidation of Si(001) surfaces completely covered with reconstructed dimers by the adsorbed O_2 molecules is obtained to be 60.4 kcal/mol by the elaborate calculations using the Møller-Plesset perturbation theory up to the second order. Some experiments exist which support this theoretical result. The temperature dependence of the reaction-rate constants was calculated theoretically on this oxidation process by considering the contribution of the quantum-mechanical tunneling effect. The apparent activation energy estimated from the Arrhenius plot with the calculated rate constants is 40 kcal/mol at low temperatures. Therefore, it was concluded that Si(001) surfaces perfectly covered with the reconstructed dimers are inert against the oxidation by the O_2 molecule at room temperature. STM images of Si(001) surfaces after an exposure of O_2 molecules support this conclusion; i.e., the oxidation by O_2 molecules starts at the defect sites only, and the reconstructed dimers remain unreactive. Natural oxides covering Si(001) surfaces might originate from the oxidation which begins at the defect sites of the surface by the O_2 molecule.

[1]U. Hofer, A. Puschmann, D. Coulman, and E. Umbach, Surf. Sci. **211/212**, 948 (1989).

[2]U. Hofer, P. Morgen, W. Wurth, and E. Umbach, Phys. Rev. B **40**, 1130 (1989).

[3]G. Hollinger, J. F. Morar, F. J. Himpsel, G. Hughes, and J. L. Jordan, Surf. Sci. **168**, 609 (1986).

[4]E. G. Keim and A.V. Silfhout, Surf. Sci. **186**, L557 (1987).

[5]W. Ranke and Y. R. Xing, Surf. Sci. **157**, 353 (1985).

[6]T. Miyake, S. Soeki, H. Kato, T. Nakamura, and A. Namiki, Phys. Rev. B **42**, 11 801 (1990).

[7]S. Ciraci, S. Ellialtioglu, and S. Erkoc, Phys. Rev. B **26**, 5716 (1982).

[8]C. Silvestre and M. Shayegan, Phys. Rev. B **37**, 10 432 (1988); *The 19th International Conference on the Physics of Semiconductors* (Poland Academic Science, Warsaw, 1988), Vol. 1, p. 777.

[9]H. Ibach, H. D. Bruchmann, and H. Wagner, Appl. Phys. A **29**, 113 (1982).

[10]J. A. Schaefer and W. Gopel, Surf. Sci. **155**, 535 (1985).

[11]L. Incoccia, A. Balerna, S. Cramm, C. Kunz, F. Senf, and I.

Storjohann, Surf. Sci. **189/190**, 453 (1987).

[12]D. Schmeisser, Surf. Sci. **137**, 197 (1984).

[13]V. Barone, Surf. Sci. **189/190**, 106 (1987).

[14]P. V. Smith and A. Wander, Surf. Sci. **219**, 77 (1989).

[15]Y. Miyamoto, A. Oshiyama, and A. Ishitani, Solid State Commun. **74**, 343 (1990); Y. Miyamoto and A. Oshiyama, Phys. Rev. B **41**, 12 680 (1990).

[16]See, for example, A. Szabo and N. S. Ostlund, *Modern Quantum Chemistry* (MacMillan, London, 1982); R. McWeeny, *Method of Molecular Quantum Mechanics*, (Academic, London, 1989).

[17]See, for example, H. B. Schlegel, *Ab Initio Methods in Quantum Chemistry I*, edited by K. P. Lawley, Advances in Chemical Physics Vol. 67 (Wiley, Chichester, 1987), pp. 249–286.

[18]M. Tsuda, T. Hoshino, S. Oikawa, and I. Ohdomari, Phys. Rev. B **44**, 11 241 (1991).

[19]T. Hoshino, M. Tsuda, S. Oikawa, and I. Ohdomari, Surf. Sci. Lett. **291**, L763 (1993).

[20]T. Hoshino, M. Tsuda, S. Oikawa, and I. Ohdomari, in *Control of Semiconductor Interfaces* (Elsevier, Amsterdam, 1994), pp. 221–226.

[21]M. S. Gordon, J. S. Binkley, J. A. Pople, W. J. Pietro, and W. J. Hehre, J. Am. Chem. Soc. **104**, 2797 (1982).

[22]T. Hoshino, S. Oikawa, M. Tsuda, and I. Ohdomari, Phys. Rev. B **44**, 11 248 (1991).

[23]K. P. Huber and G. Herzberg, *Library of Congress Cataloging in Publication Data—Molecular Spectra and Molecular Structure* (Van Nostrand Reinhold, New York, 1979).

[24]S. Oikawa and M. Tsuda, J. Am. Chem. Soc. **107**, 1940 (1985).

[25]W. Jakubetz, J. Am. Chem. Soc. **101**, 298 (1979).

[26]R. J. L. Roy, H. Murai, and F. Williams, J. Am. Chem. Soc. **102**, 2325 (1980).

[27]C. Eckart, Phys. Rev. **35**, 1303 (1930).

[28]E. F. Caldin, Chem. Rev. **69**, 135 (1969).

[29]J. R. Engstrom, M. M. Nelson, and T. Engel, J. Vac. Sci. Technol. A **7**, 1837 (1989).

[30]J. R. Engstrom and T. Engel, Phys. Rev. B **41**, 1038 (1990).

[31]M. P. D'Evelyn, M. M. Nelson, and T. Engel, Surf. Sci. **186**, 75 (1987).

[32]M. L. Yu and B. N. Eldridge, Phys. Rev. Lett. **58**, 1691 (1987).

[33]K. Ohkubo, Y. Igari, S. Tomoda, and I. Kusunoki, Surf. Sci. **260**, 44 (1992).

[34]T. Hoshino, M. Tsuda, S. Oikawa, and I. Ohdomari, in *Interface Control of Electrical, Chemical, and Mechanical Properties*, MRS Symposia Proceedings No. 318 (Materials Research Society, Pittsburgh, 1994).

[35]Ph. Avouris and I. W. Lyo, Appl. Surf. Sci. **60/61**, 426 (1992).

[36]F. Bozso and Ph. Avouris, Phys. Rev. B **44**, 9129 (1991).

[37]T. Sunada, T. Yasaka, M. Takakura, S. Miyazaki, and M. Hirose, Jpn. J. Appl. Phys. **29**, 2408 (1990).
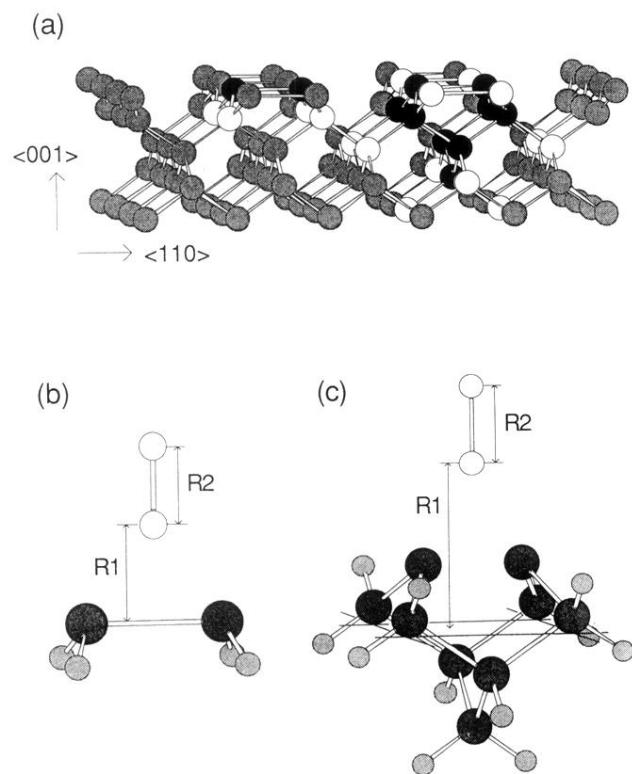
(a)

<001>

<110>

(b)

R2

R1

(c)

R2

R1

FIG. 1. (a) 2×1 reconstructed Si(001) surface. Solid and open spheres at the left were considered for the construction of a small model, and those at the right for a large model. (b) A molecular system of the small model, $Si_2H_4 + O_2$. (c) A molecular system of the large model, $Si_9H_{12} + O_2$. Large and small solid spheres denote silicon and hydrogen atoms, respectively. Open spheres denote oxygen atoms in (b) and (c).

8.0
(1.0)
1.24Å
8.0
(1.0)
4.30Å
13.7
(0.0)
1.1
(0.0)

(a) Shallow Minimum

8.1
(1.7)
1.65Å
8.2
(0.7)
2.12Å
13.7
(-0.2)
1.1
(0.0)

(b) Transition State

8.0
(2.0)
2.66Å
8.9
(0.0)
1.37Å
13.2
(0.0)
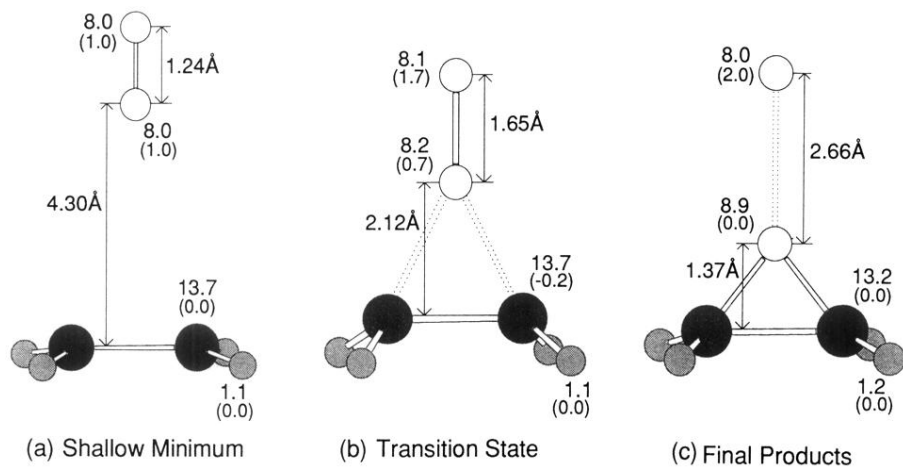1.2
(0.0)

(c) Final Products

FIG. 4. Atomic configurations for (a) the shallow minimum, (b) the transition state, and (c) the final stable state of the oxide in the spin triplet state, which correspond to (a), (b), and (c), respectively in Fig. 3. Electron densities and alpha spin densities (in parentheses) obtained by Mulliken population analysis are also shown.
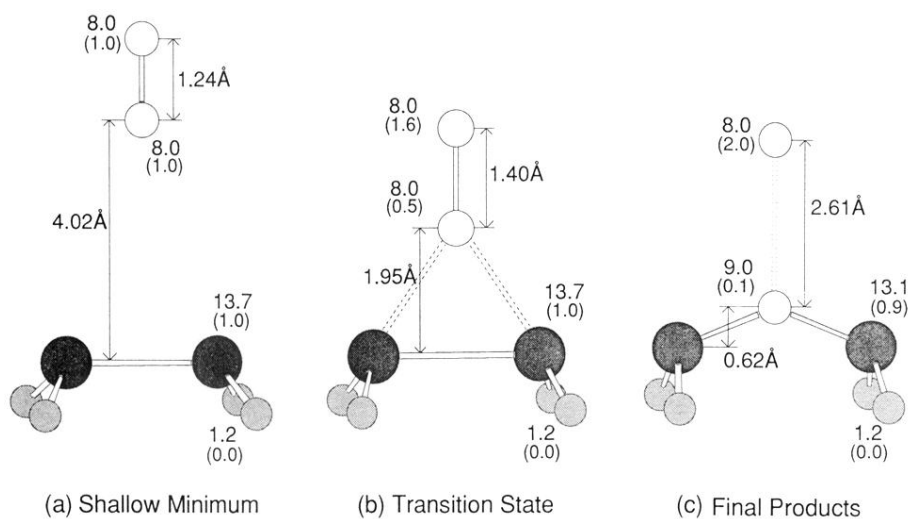
FIG. 6. Atomic configurations for (a) the shallow minimum, (b) the transition state, and (c) the final stable state in the spin quintet state, which correspond to (a), (b), and (c) in Fig. 5, respectively. Electron densities and alpha spin densities (in parentheses) obtained by Mulliken population analysis are also shown.